M^{2+} doping induced simultaneous phase/size control and remarkable enhanced upconversion luminescence of $NaLnF_4$ probes for optical-guided tiny tumor diagnosis

Youbin Li, Xiaolong Li, Zhenluan Xue, Mingyang Jiang, Songjun Zeng, and Jianhua Hao**

Prof. S. J. Zeng, Y. B. Li, Z. L. Xue, X. L. Li, M. Y. Jiang
College of Physics and Information Science and Key Laboratory of Low-dimensional Quantum Structures and Quantum Control of the Ministry of Education, Hunan Normal University, Changsha, 410081, China.
E-mail: songjunz@hunnu.edu.cn
Prof. J. H. Hao
Department of Applied Physics and Materials Research Center, The Hong Kong Polytechnic University, Hong Kong.
E-mail: jh.hao@polyu.edu.hk

Keywords: M^{2+} doping, phase/size control, cubic to hexagonal phase transformation, optical-guided tiny tumor diagnosis

Doping has played a vital role in constructing desirable hybrid materials with tunable functions and properties via incorporating atoms into host matrix. Herein, a simple strategy for simultaneously modifying the phase, size and upconversion luminescence (UCL) properties of the $NaLnF_4$ (Ln = Y, Yb) nanocrystals by high-temperature co-precipitation through non-equivalent M^{2+} doping (M=Mg^{2+}, Co^{2+}) has been demonstrated. The phase transformation from cubic to hexagonal was readily achieved by doping M^{2+}. Compared with Mg-free sample, a remarkable enhancement of overall UCL (~27.5 times) was obtained by doping Mg^{2+}. Interestingly, owing to the efficient UCL, red UCL-guided tiny tumor (down to 3 mm) diagnosis was demonstrated for the first time. Our results open up a new way of designing high efficient UCL probe with combination of hexagonal and small size for tiny tumor detection.

1. Introduction

Lanthanide-doped upconversion nanoparticles (UCNPs) have triggered considerable interests as biological imaging probes for their unique UCL properties of exhibiting high energy shorter wavelengths emission under continuous near-infrared (NIR) excitation.[1-5] In contrast with the conventional organic fluorophores and semiconducting quantum dots, UCNPs can significantly minimize autofluorescence of biosamples, decrease the photodamage, and possess large penetrating depth in biotissue through NIR excitation, making them highly suitable for bioimaging probes.[1f,1g,6-7] As an optimal biological nanoprobe, bright UCL and small diameter are rigorously required for the nanocrystalline.[8] Therefore, it is important for us to synthesize small sized nanocrystals with intense UCL under the excitation of NIR.

Among all of the developed UCL hosts, $NaLnF_4$ system was considered as the most efficient UCL host. $NaLnF_4$ system usually possesses two phase structures, cubic and hexagonal, and the UCL efficiency of hexagonal phase $NaYF_4$ is an order of magnitude UCL intension strengthen than that of the cubic phase.[9] However, sufficiently high temperature and longstanding treatment are required to form the pure hexagonal phase structure, subsequently resulting in the increase of particle size.[1b] Moreover, precisely adjusting some important parameters including the nature of the solvent, temperature and reaction time,[1a,10] are required for the conventional methods to control the structure of UCNPs, leading to a complicated experimental process. It is a great challenge to synthesize high efficient UCNPs in combination of hexagonal phase and small size. Therefore, it is of great significance to develop a convenient method to control the crystal phase and size of UCNPs. Recently, Liu's group has demonstrated a simple lanthanide doping method for simultaneous phase and size control of $NaLnF_4$ system.[1b] Li's group reported the sub-10 nm hexagonal $NaLuF_4$ UCNPs with efficient UCL and sensitive *in vivo* bioimaging by doping Gd^{3+}.[1a] Our previous report also demonstrated the bi-functional $NaLuF_4$ UCNPs with controlled structures and tunable

magnetic properties by doping Gd^{3+}.[3f] Very recently, Zhao[11a] and our previous reports[11b] proposed a transition metal Mn^{2+} doping method for simultaneous phase and size control of $NaLnF_4$ nanocrystals by oleic acid assistant hydrothermal method. Liu and co-workers also demonstrate that the lanthanide doping induced shape/size control of alkaline-earth fluoride nanocrystals (SrF_2) and M^{2+} (Ba^{2+}, Sr^{2+}) doping can promote the crystal growth and increase the particle size in LnF_3 (Ln=Ce, La) host.[12] Inspired by these results, we propose that the non-equivalent M^{2+} ion substitution of Ln^{3+} in $NaLnF_4$ host may also promote the particle growth and finally realize the cubic to hexagonal phase transformation at high temperature by thermal-decomposition method.

Here, as a proof of concept, we have synthesized the $NaLnF_4$ UCNPs with simultaneous control of the phase and size by a simple M^{2+} (Mg^{2+}, Co^{2+}) doping method. The as-synthesized $NaLnF_4$ UCNPs with obvious phase transformation and small sized hexagonal phase structure were performed by a modified high-temperature co-precipitation method for short reaction time of 25 min at the temperature of 305 ℃ by doping M^{2+}. More importantly, *in vivo* red UCL bioimaging and tiny tumor detection were conducted by using the $NaYF_4$: Yb/Er/Mg UCNPs.

2. Results and Discussion

2.1. Doping Induced Phase/Size Control

The as-prepared $NaYF_4$:20%Yb/2%Er UCNPs with different contents of Mg^{2+} were first analyzed by X-ray diffraction patterns（XRD）patterns (**Figure 1**). As shown in the Figure 1, Mg-free UCNPs exist both the cubic (JCPDS file number 77-2043) and hexagonal phase (JCPDS file number 16-0334) particles. Notably, when doping 10% Mg^{2+}, pure hexagonal phase UCNPs were achieved. And no other extra diffraction peaks were observed when continuously increasing the doping contents of Mg^{2+} up to 20%, indicating the successful incorporation of Mg^{2+} into the host matrix and formation of a homogeneous Y-Mg solid

solution structure. In addition, the diffraction peak gradually shift to higher angle as a function of Mg^{2+} contents, which is attributed to the decrease of unit-cell volume induced by the substitution of Y^{3+} (r=1.159)[13] ions by the smaller Mg^{2+} [13] ions. These findings reveal that the Mg^{2+} doping can promote the cubic to hexagonal phase transformation. It should be pointed out that the complete phase conversion from cubic to hexagonal phase only takes 25 minutes at 305 C.

To further reveal the phase/size control, $NaYF_4$:Yb/Er UCNPs doped with different contents of Mg^{2+} were performed by transmission electron microscopy (TEM) (**Figure 2**). Without the present of Mg^{2+} ions, the TEM image (Figure 2a) of $NaYF_4$ UCNPs consist of two kinds of particle morphologies that include the large nanoparticles (sub-15 nm) and ultra-small ones (sub-5 nm). And the detected selected-area electron diffraction (SAED, Figure 2b) reveal the ultra-small particles were face-centered cubic phase structure, which is well consistent with the analysis result of XRD in the absence of Mg^{2+}. By adjusting the doping concentration of Mg^{2+}, as demonstrated in Figure 2c, Figure 2d, and Figure 2e, highly uniform and monodispersity pure hexagonal phase $NaYF_4$:Yb/Er/Mg UCNPs were obtained. The size of UCNPs tuned from 5-40 nm by adjusting the content of Mg^{2+}. High-resolution TEM (HRTEM, Figure 2f) of a single particle taken from Figure 2d shows the high crystallization nature and its interplanar crystal space is estimated to be 5.14 , matching well with the (100) crystal plane of hexagonal phase $NaYF_4$ UCNPs. The SAED result of $NaYF_4$:Yb/Er/Mg UCNPs (Figure 2g) reveal the formation of pure hexagonal phase structure, further verifying the phase transformation from cubic to hexagonal. Furthermore, energy dispersive X-ray spectrometer (EDS) analysis (Figure 2h) taken from Figure 2d elucidate the presence of Na, Y, F, and the doped Yb, Mg elements.

As demonstrated in **Scheme 1**, upon addition of Mg^{2+} ions, the non-equivalent M^{2+} ion substitution of Y^{3+} in $NaYF_4$ system can form positive vacancies on the particle surface for charge balance, which subsequently forms transient electric dipoles with positive poles

pointing outward.[12] Therefore, the absorption of F^- from the solution to the grain surface is remarkably enhanced,[12] promoting the crystal growth of $NaYF_4$ UCNPs and finally resulting in cubic to hexagonal phase conversion.

To further elucidate the possibility of M^{2+} doping induced phase/size control, $NaYF_4$ UCNPs doped with different concentrations of Co^{2+} were synthesized under the same method. As shown in **Figure 3**, similar to those of Mg^{2+}, the Co-free sample consists of two phase, cubic and hexagonal phase. Notably, the obvious phase conversion from cubic to hexagonal is also achieved by doping Co^{2+}. When doping 20 mol% Co^{2+}, all of the diffraction peaks were matched well with the pure hexagonal phase structure, indicating the completed phase transformation from cubic to hexagonal. TEM results (**Figure 4**) also demonstrate that the small cubic UCNPs are gradually decreased and converted to the larger well dispersed hexagonal phase $NaYF_4$ UCNPs (~15 nm) by increasing the contents of Co^{2+}. These findings reveal that our proposed non-equivalent M^{2+} doping is a general method for designing phase/size controlled nanostructure.

To shed more light on the versatility of the proposed M^{2+} doping method, we have prepared some related $NaLnF_4$ UCNPs. For example, different contents of Co^{2+} doped $NaYbF_4$ UCNPs were prepared by using the same method. Obviously, the phase and size control of $NaYbF_4$ UCNPs by doping with Co^{2+} was in accordance with the case of $NaYF_4$ UCNPs, as shown in Figure S1, Figure S2. As proved in Figure S1, Co-free and 5% Co^{2+} doped $NaYbF_4$ UCNPs presented the pure cubic phase structure. Pure hexagonal phase $NaYbF_4$ UCNPs were obtained when we increased the Co^{2+} to 40%. As demonstrated in Figure S2, TEM result reveals that the sample with absence of Co^{2+} and 5% Co^{2+} only present cubic particles, and pure larger hexagonal phase $NaYbF_4$ UCNPs are obtained when increasing the content of Co^{2+} up to 40%, further proving the simultaneously modifying of phase and size of $NaLnF_4$ host by M^{2+} doping.

In addition, from the XRD and TEM results, it is noted that Mg^{2+} can lead the phase transformation more easily than Co^{2+}. We speculate that the Mg^{2+} ions are more easily incorporated into host matrix at the same nominal doping concentrations in comparison to Co^{2+}. To further reveal the actual doping contents of M^{2+} in host matrix, quantity EDS analysis was performed**.** As shown in **Table S1**, the actual M^{2+} content doped into host matrix was relatively lower than the nominal concentration. Moreover, when doping the same nominal concentrations of Mg and Co ions (20%), the actual content of Mg^{2+} in host matrix is reached to 11.3%, which is higher than Co^{2+} (4.9%), indicating that the Mg^{2+} is comparatively easy to be incorporated into the $NaLnF_4$ host matrix at the same doping concentration. Therefore, compared with Co^{2+}, the more contents of Mg^{2+} incorporated into $NaLnF_4$ host matrix can graft more F^- ions onto the grain surface, subsequently improving the cubic to hexagonal phase conversion. According to the previous reports[3i, 14], it is expected that the UCL intensity can be further improved by doping A^+ ions (Li^+ or K^+) for charge compensation.

2.2. Remarkable Enhancement of UCL

To reveal the impact of M^{2+} doping on UCL properties, the UCL spectra of Mg^{2+} doped $NaYF_4$: Yb/Er UCNPs were studied. As demonstrated in **Figure 5**, the UCL intensity was sharply enhanced by doping Mg^{2+}. Compared with the Mg-free UCNPs, the overall UCL intensity of UCNPs doped with 20% Mg^{2+} is enhanced by ~27.5 times. The vividly digital photographs (insets of the Figure 5b) exhibit gradually enhanced intensity of eye-visible green UCL, matching well with the UCL spectra. The strong green emission bands centered at 520/545 nm and relatively weak red UCL on 664 nm are assigned to the $^2H_{11/2}$ / $^4S_{3/2}$ – $^4I_{15/2}$ and $^4F_{9/2}$ – $^4I_{15/2}$ electronic transitions of Er^{3+}, respectively (Figure 5a). As shown in UCL spectra, the $NaYF_4$ UCNPs doped with Mg^{2+} presented the dominant green and relatively weak red emissions, and the red to green ratio was not changed by doping Mg^{2+}, which is

different with Mn^{2+} doped UCNPs[11a,b] and consistent well with the result of the previous report[3h], indicating no obvious energy transfer from Mg^{2+} /Co^{2+} to rare earth ions.

2.3. Cell cytotoxicity test

The biocompatibility of the as-synthesized Mg-doped $NaYF_4$: Yb/Er UCNPs was tested by using 3-(4, 5-dimethylthiazol-2-yl)-2,5-diphenyl-tetrazolium bromide (MTT) method in HeLa cells (Figure S3). As demonstrated, the cell viability of these UCNPs in HeLa cells was 98.36% when dealing with 100 μg/mL UCNPs. When the concentrations of these UCNPs increased to 1000 μg/mL, the cellular viability was still estimated to be 89.18%, indicating the low cytotoxicity of these ligand-free UCNPs. Therefore, the ligand-free UCNPs simultaneously possess remarkable UC emission and low cytotoxicity, making it ideal nano-probe for *in vivo* optical bioimaging.

2.4. *In Vivo* upconversion imaging

It is well known that optical nanoprobes with emission peaks located at "biological transparent window [15] (650-1000 nm)" are more suitable for *in vivo* optical bioimaging because of its low tissue absorption and large penetrating depth. Although, UCNPs exhibit intense eye-visible green UCL, the red UCL is also remarkably enhanced by 20.1 times, which is more applicable as bio-probe.[11, 16] Prior to *in vivo* bioimaging applications, the hydrophobic $NaYF_4$ UCNPs were first converted into hydrophilic ones by using HCl treating method[17]. The *in vitro* UCL imaging detected at red region (**Figure 6**b) revealed that the Mg doped UCNPs presented significant enhancement of optical signal, compared with Mg-free sample. In addition, *in vivo* UCL whole body bioimaging of Kunming mouse at different time intervals after intravenously injected with 20%mol Mg doped $NaYF_4$ UCNPs was performed. As demonstrated in Figure 6, UCL signals were mainly focused in the liver and spleen after 1 h injection. The UCL signal was gradually enhanced after 5 h injection and tend to slight

decrease after 7 h, matching well with our previous reports[18]. The weak UCL signal can be detected until 24 h later. UCL signal distribution and translocation of UCNPs were further studied through *ex-vivo* imaging. The injected mouse was dissected to acquire the isolated organs including heart, liver, spleen, lung, and kidney for UCL signal detection. As proved in Figure 6c, UCL signals of the isolated organs was mainly focused in the liver, spleen, and relatively weaker signal was detected in the lung, which showed same distribution trend compared with the live mouse. The result reveals that the UCNPs with enhanced red UCL are also ideal probes for *in vivo* deep-tissue bioimaging.

2.5. UCL bioimaging-guided tiny tumor diagnosis

In vivo Detection of tiny tumor is of great significant for early clinic cancer diagnosis. Nevertheless, the tiny tumor (under 5 mm) possesses a lower uptake of macromolecular drugs and dramatic comparable geometric resistances compared with the large one.[19a] Therefore, it is a great challenge for the probes to be accumulated in the tiny tumor at a high blood flow rate.[19a] There are reports that the enhanced permeability and retention (EPR) effect can lead to efficient diffusion of probes from the tumor vasculature and retention in the tumor site. The size of the probes is proposed ranging from 20 nm to 200 nm,[19b] which are not only required small enough to escape from tumor vasculature cells and selectively accumulating in the tumor site, but also large enough to avoid being clearance from the kidney tissue.[19b, 19c] Therefore, it is expected that our designed red UCL Mg-doped $NaYF_4$:Yb/Er UCNPs with size of 35 nm can be used as optical probes for high sensitive tiny-tumor detection.

To validate the possible application for tiny tumor diagnosis, *in vivo* red UCL-guided bioimaging of tumor bearing mouse treated with these UCNPs was performed. As demonstrated in **Figure 7**a, after 1 h injection, UCL signals are mainly observed in the liver and spleen, which is well consistent with the aforementioned result. Subsequently, UCL signal in the tumor site is detected after 3 h injection and gradually increased until 8 h injection, indicating the effective accumulation of UCNPs in tumor via EPR effect. Moreover,

it is noted that the UCL signal can be still observed after 12 h injection, indicting the feasibility of long-time visualization of tumor. To further reveal the sensitive detection of tiny tumor, *ex-vivo* UCL images of the tiny tumor was conducted. As presented in Figure 7c, intense UCL signal was observed in the tumor site. The results demonstrate that the UCNPs can be effectively accumulated in the tumor site, making it desirable optical nanoprobe for tiny tumor detection.

3. Conclusion

In summary, a strategy of M^{2+} doping for simultaneous phase/size control and enhanced UCL of hexagonal $NaLnF_4$ UCNPs are first demonstrated via a modifying high-temperature co-precipitation method. These UCNPs exhibit tunable UCL emission, making them highly suitable for bioimaging. For the first time, we have successfully realized the red UCL-guided diagnosis of tiny tumor (~ 3 mm), which open up a new way for the design of bright UCL probe for further application in deep tissue bioimaging and early cancer diagnosis.

4. Experimental Section

Chemicals and materials: All chemical reagents were obtained from commercial supplies and used without further purification. Rare earth $YbCl_3•6H_2O$ (99.99%), $TmCl_3•6H_2O$ (99.99%), $ErCl_3•6H_2O$ (99.99%), $YCl_3•6H_2O$ (99.99%) were purchased from QingDa elaborate Chemical Reagent Co. Ltd (Shandong). Oleic acid (OA, 90%) was purchased from Sigma-Aldrich. 1-octadecene (90%) was supplied by Xi ya Chemical Reagent Co. Ltd. NaOH (96%) was purchased from Sinopharm Chemical Reagent Co. Ltd (Shanghai). NH_4F (96.0%) was purchased from Xi Long Chemical Reagent Co. Ltd. CH_4OH (99.5%) was supplied by JinFeng Chemical Reagent Co. Ltd. $MgCl_2•6H_2O$ (98.0%) and $CoCl_2•6H_2O$ (99.0%) were purchased from HengXing Chemical Reagent Co. Ltd. (Tianjin)

Synthesis of $NaLnF_4$ (Ln = Y, Yb) UCNPs: The Mg^{2+} doped $NaYF_4$ UCNPs were synthesized by a modified high-temperature co-precipitation procedure[20] as follows: $YbCl_3$ and YCl_3,

$ErCl_3$ and $MgCl_2$ at varied ratios with a total lanthanide amount of 2 mmol were added to a 100 mL three-neck flask containing oleic acid (12 mL) and 1-octadecene (30 mL). The mixture was heated at 160 ℃for 1 h to remove the total oxygen and remaining water. Subsequently, the temperature was cooled down to 90 ℃. 0.296 g NH_4F and 0.2 g NaOH were dissolved respectively in 10mL/20 mL of methanol, respectively and simultaneously and slowly added into the reaction flask in 20 min. The solution was stirred for 1h at room temperature, then the mixture solution was heated to 60 ℃ and stirred for another 1 h. After removing methanol, the solution was heated to 305 ℃ and maintained under argon flow for 25 min, and then was cooled down to room temperature. The resulting UCNPs were precipitated by the addition of ethanol, collected by centrifugation, washed with cyclohexane and ethanol several times, and finally dispersed in 5 mL of cyclohexane. The synthesized method of other $NaLnF_4$ UCNPs, for example, $NaYF_4$:20Yb/2Er/xCo mol% (x= 5, 10, 20) and $NaYbF_4$:2Tm/xCo mol% (x= 0, 5, 10, 20, 30, 40) were the same to the Mg doped $NaYF_4$ UCNPs.

Synthesis of hydrophilic $NaLnF_4$ (Ln = Y, Yb) UCNPs: The hydrophilic Mg-free $NaYF_4$ UCNPs and 20% Mg doped $NaYF_4$ UCNPs were prepared for *in vivo* bioimaging by using a HCl treated method[17]. In a typical process, OA-$NaYF_4$ UCNPs (1 mmol) were dispersed in 10 mL aqueous solution. Then a HCl solution with concentration of 0.1 M was added, and the pH value was adjusted at 3.2 under vigorously stirring. After that, the mixture was stirred for 2 h. After the reaction was completed, the ligand-free UCNPs in the water were collected by centrifugation and washed with deionized water for at least three times. Finally, the solution was dispersed in deionized water for further used as contrast agents.

Cytotoxicity assay: The *in vitro* cell viability of ligand-free $NaYF_4$: Yb/Er/Mg UCNPs in HeLa cells was measured via a MTT proliferation assay method. Firstly, HeLa cells were transferred into a 96-well microplate (6000 cells per well) and cultured at 37 ℃ under 5%

CO_2 for 3h. Then the cell culture medium in each well was replaced by Dulbecco's Modified Eagle Medium (DMEM) solution including 10% fetal bovine serum, 1% penicillin and streptomycin and different concentrations of $NaYF_4$:Yb/Er/Mg UCNPs (10, 50, 100, 200, 300, tem500, 1000 μg/ mL) at 37 °C and with 5% CO_2 for another 20 h. A typical MTT assay was used to calculate the cell viability.

Characterization: The crystal phase of the samples were recorded by a Rigaku D/max 2500 system X-ray diffractometer (XRD) with Cu-Ka radiation A . 54 6 nm at 4 kV and 25 mA. The morphologies and size of the as-prepared samples were characterized by transmission electron microscopy (TEM, FEI Tecnai F20) equipped with the energy dispersive X-ray spectroscopy (EDS, Oxford Instrument) system using an accelerating voltage of 200 kV. The UCL spectra were detected by a Zolix spectrophotometer (fluoroSENS 9000A) equipped with an external 980 nm laser as light source at room temperature. The digital photos of the $NaYF_4$ UCNPs were taken by canon digital camera under the excitation of 980 nm laser.

UCL optical bioimaging: The $NaYF_4$:Yb/Er UCNPs and $NaYF_4$:Yb/Er/Mg UCNPs were first added in the 96-well plates (300 μL per well) with same concentration (3 mg/mL), respectively. *In vitro* phantom UCL bioimaging was collected by *in vivo* imaging system (Bruker *In Vivo* FX Pro) installed with 980 nm laser as light source. UCL signal was acquired by the band pass filter (670/20 nm). For *in vivo* imaging, a Kunming mouse was injected with pentobarbital sodium aqueous (200 μL/10 wt%) for *in vivo* bioimaging. 200 μL of aqueous solution containing $NaYF_4$:Yb/Er/Mg UCNPs (3 mg/mL) was injected into the mouse through intravenous injection at tail vein. *In vivo* UCL bioimaging was collected by the same imaging system. All animal procedures comply with the institutional animal use and care regulations approved by the Laboratory Animal Center of Hunan Province

UCL optical bioimaging of tiny tumor diagnosis: 8×10^6 MAT-Ly-Lu-B-2 (Mat) cells were subcutaneously injected into the BALB/C mouse for further culturing the tumor to about ~3

mm in average size. The inoculated tumor mouse was primarily anesthetized by intraperitoneal injection with 150 μL/10 wt% pentobarbital sodium aqueous. 300 μL of hydrophilic $NaYF_4$:20Yb/2Er/20Mg mol% UCNPs (3 mg/mL) was then injected into the mouse via intravenous injection. The UCL optical signal was collected by *in vivo* bioimaging system (Bruker *In Vivo* FX Pro) in different time intervals from 5 min to 13 h. The emission filter was set as 670 nm, and the exposure time was set as 60 s. The *ex-vivo* signals were acquired by the same system and condition. The digital pictures of the organs were taken by Canon digital camera.

Supporting Information

Supporting Information is available from the Wiley Online Library or from the author.

Acknowledgements

This work was supported by the National Natural Science Foundation of China (No. 21671064), specialized research Fund for the Doctoral Program of Higher Education of China (No. 20114301120006), Scientific Research Fund of Hunan Provincial Education Department (13B062).

Received: ((will be filled in by the editorial staff))
Revised: ((will be filled in by the editorial staff))
Published online: ((will be filled in by the editorial staff))

[1] a) Q. Liu, Y. Sun, T. S. Yang, F. Wang, C. G. Li, F. U. Li, *J. Am. Chem . Soc.* **2011**, *133*, 17122; b) F. Wang, Y. Han, C. S. Lim, Y. H. Lu, J. Wang, J. Xu, H. Y. Chen, C. Zhang, M.H. Hong, X. G. Liu, Nature **2010**, *463*, 1061; c) F. Auzel, *Chem. Rev.* **2004**, *104*, 139; d) X. M. Li, F. Zhang, D. Y. Zhao, *Chem. Soc. Rev.* **2015**, *44*, 1346; e) F. Wang, X. G. Liu, *Chem. Soc. Rev*. **2009**, *38,* 976; f) J. Zhou, Z. Liu, F. Y. Li, *Chem. Soc. Rev*. **2011**, *41*, 1323; g) D. M. Yang, P. A. Ma, Z. Y. Hou, C. X. Li, J. Lin, *Chem. Soc. Rev*. **2015**, *44*, 1416; h) Z. Q. Li, Y. Zhang, S. Jiang, *Adv Mater*. **2008**, *20*, 4765; i) C. Chen, C. Li, Z. Shi, *Adv. Sci.* **2016**, *3*,

1600029; j) F. Li, C. Li, X. Liu, Y. Chen, T. Bai, L. Wang, Z. Shi, S. Feng, *Chem.- Eur. J.* **2012**, *18*, 11641.

[2] a) R. Parthiban, C. Prakash, W. R. Seog, K. Jinkwon, *Nanoscale* **2013**, *5*, 8711; b) Riya, K.R. Deya an Vineet, *Dalton Trans* **2014**, *43*, 111; c) A. Hassane, S. Guo-Bin, D. Nathan, P. George, *Demopoulos Cryst Eng Comm* **2013**, *15*, 4739; d) H. T. Wong, M. K. Tsang, C. F. Chan, K. L. Wong, B. Fei, J. H. Hao, *Nanoscale* **2013**, *5*, 3465; e) P. Huang, F. Liu, D. Q. Chen, Y. S. Wang, Y. L. Yu, *phys. stat. sol*. **2008**, *205*, 1680; f) Y. F. Wang, L. D. Sun, J. W. Xiao, W. Feng, J. C. Zhou, J. Shen, C. H. Yan, *Chem. Eur. J*. **2012**, *18*, 5558; g) G. F. Wang, Q. Peng, Y. D. Li, *J. Am. Chem. Soc*. **2009**, *131*, 14200; h) N. M. Idris, Z. Q. Li, L. Ye, E. K. W. Sim, R. Mahendran, P. C. L. Ho, Y. Zhang, *Biomaterials* **2009**, *30*, 5104.

[3] a) F. Chen, W. B. Bu, S. J. Zhang, X. H. Liu, J. N. Liu, H. Y. Xing, Q. F. Xiao, L. P. Zhou, W. J. Peng, L. Z. Wang, J. L. Shi, *Adv. Funct. Mater.* **2011**, *21*, 4285; b) S. F. Helmut, P. Pavel, Z. Otmane, M. Haase, *Adv. Funct. Mater.* **2008**, *18*, 2913; c) M. Nyk, R. Kumar, T. Y. Ohulchanskyy, E. J. Ohulchanskyy, P. N. Prasad, *Nano Lett*. **2008**, *8*, 3834; d) J. Shen, L. Zhao, G. Han, *Advanced Drug Delivery Reviews* **2013**, *65*, 744; e) Q. Liu, Y. Sun, C. G. Li, J. Zhou, C. Y. Li, T. S. Yang, X. Z. Zhang, T. Yi, D. M. Wu, F. Y. Li, *ACS Nano* **2011**, *5*, 3146; f) S. J. Zeng, J. J. Xiao, Q. B. Yang, J. H. Hao, *J. Mater. Chem.* **2012**, *22*, 9870; g) J. A. Damasco, G. Y. Chen, W. Shao, H. Ågren, H. Y. Huang, W. T. Song, J. F. Lovell, P. N. Prasad, *ACS Appl. Mater. Interfaces.* **2014**, *6*, 13884; h) Q. Cheng, Y. Li, S. X. Liu, J. H. Sui, W. Cai, *RSC Adv*., **2015**, *5*, 93547; i) Q. Cheng, J. h, Sui, W. Cai, *Nanoscale*, **2012**, *4*, 779.

[4] a) L. Q. Prasad, Z. G. Chen, Q. W. Tian, T. Y. Cao, C. J. Xu, F. Y. Li, *Anal. Chem*. **2009**, *81*, 8687; b) J. L. Liu, Y. Liu, Q. Liu, C. Y. Li, L. N. Sun, F. Y. Li, *J. Am. Chem. Soc*. **2011**, *133*, 15276; c) H. T. Wong, H. L. W. Chan, J. H. Hao, *Opt. Express* **2010**, *6*, 6123; d) S. Heer, K. Kompe, H. U. Gudel, M. Haase, *Adv. Mater.* **2005**, *17*, 2119; e) N. M. Idris, M. K. G. Jayakumar, A. Bansalab, Y. Zhang, *Chem. Soc. Rev.* **2015**, *44*, 1449.

[5] a) D. K. Chatterjee, M. K. G Jayakumar, Y. Zhang, *Small* **2010**, *6*, 2781; b) X. Yu, M. Yu, M. Xie, L. Chen, Y. Li, Q. Wang, *Nano Res*. **2010**, *3*, 51; c) Z. G. Chen, H. L. Chen, H. Hu, M. X. Yu, F. Y. Li, Q. Zhang, Z. G. Zhou, T. Yi, C. H. Huang, *J. Am. Chem. Soc*. **2008**, *130*, 3023.

[6] a) M. X. Yu, F. Y. Li, Z. G. Chen, H. Hu, C. Zhan, C. H. Huang, *Anal. Chem*. **2009**, *81*, 930; b) M. Wang, C. C. Wang, W. X. Wang, C. H. Liu, Y. F. Wu, Z. R. Xu, C. B. Mao, K. S. Xu, *ACS Nano 2009*, *3*, 1580; c) Z. L. Wang, J. H. Hao, H. L. W. Chan, G. L. Law, W. T. Wong, K. L. Wong, M. B. Murphy, T. Su, Z. H. Zhang, S. Q. Zeng, *Nanoscale*. **2011**, *3*, 2175.

[7] a) D. K. Chatterjee, A. J. Rufaihah, Y. Zhang, *Biomaterials*, **2008**, *29*, 937; b) J. Zhou, Y. Sun, X. X. Du, L. Q. Xiong, H. Hu, F. Y. Li, *Biomaterials* **2010**, *31*, 3287.

[8] H. Kobayashi, M. Ogawa, R. Alford, P. L. Choyke, Y. Urano, *Chem. Rev*. **2010**, *110*, 2620.

[9] a) G. S. Yi, G. M. Chow, *Adv. Funct. Mater*. **2006**, *16*, 2324; b) K. W. Krämer, D. Biner, G. Frei, H. U. Güdel, M. P. Hehlen, S. R. Hehlen, *Chem. Mater.* **2004**, *16*, 1244.

[10] a) X. Wang, J. Zhuang, Q. Peng, Y. Li, *Nature* **2005**, *437*, 121; b) H. Mai, *J. Am. Chem. Soc*. **2006**, *128*, 6426; c) Y. Chen, M. Kim, G. Lian, M. B. Johnson, X. Peng, *J. Am. Chem.Soc*. **2005**, *127*, 13331; c) J. C. Boyer, F. Vetrone, L. A. Cuccia, J. A. Capobianco, *J. Am. Chem. Soc.* **2006**, *128*, 7444.

[11] a) G. Tian, Z. Gu, L. Zhou, W. Yin, X. Liu, L. Yan, S. Jin, W. Ren, G. Xing, S. Li, Y. L. Zhao, *Adv. Mater.* **2012**, ***24***, 1226; b) S. J. Zeng, Z. G. Yi, W. Lu, C. Qian, H. B. Wang, L. Rao, T. M. Zeng, H. R. Liu, H. J. Liu, B. Fei, J. H. Hao, *Adv. Funct. Mater.* **2014**, *26*, 4051.

[12] D. Q. Chen, Y. L. Chen, F. Huang, P. Huang, P. A. Yang, Y. S. Wang, *J. Am. Chem. Soc*. **2010**, *132*, 9976.

[13] R. D. Shannon, *Acta Crystallogr. A* **1976**, *32*, 751.

[14] W. Zheng, S. Y. Zhou, Z. Chen, P. Hu, Y. S. Liu, D. T. Tu, H. M. Zhu, R. F. Li, M. D. Huang, X. Y. Chen, *Angew. Chem. Int. Ed.* **2013**, *52*, 6671.

[15] a) G. Y. Chen, T. Y.; Ohulchanskyy, R. Kumar, H. Ågren, P. N. Prasad, *ACS Nano* **2010**, *4*, 3163; b) Z. G. Yi, X. L. Li, Z. L. Xue, X. Liang, W. Lu, H. Peng, H. R. Liu, S. J. Zeng, J. H. Hao, *Adv. Funct. Mater*. **2015**, *46*, 7119.

[16] a) J. Wang, F. Wang, C. Wang, Z. Wang, X. G. Liu, *Angew. Chem. Int. Ed.* **2011**, *50*, 10369; b) M. Wu, E. H. Song, Z. T. Chen, S. Ding, S. Ye, J. J. Zhou, S. Q. Xu, Q. Y. Zhang, *J. Mater. Chem. C*, **2016**, *4*, 1675.

[17] N. Bogdan, F. Vetrone, G. A. Ozin, J. A. Capobianco, *Nano Lett.* **2011,** *11*, 835.

[18] a) S. J. Zeng, H. B. Wang, W. Lu, Z. G. Yi, L. Rao, H. R. Liu, J. H. Hao, *Biomaterials* **2014**, *35*, 2934; b) Z. G. Yi, W. Lu, Y. R. Xu, J. Yang, L. Deng, C. Qian, T. M. Zeng, H. B. Wang, L. Rao, H. R. Liu, S. J. Zeng, *Biomaterials* **2014**, *35*, 9689.

[19] a) C. Y. Liu, Z. Y. Gao, J. F. Zeng, Y. Hou, F. Fang, Y. L. Li, R. R. Qiao, L. Shen, H. Lei, W. S. Yang, M. Y. Y. Gao, *ACS Nano,* **2013**, *7*, 7227; b) P. P. Adiseshaiah, J. B. Hall, S. E. McNeil, *Nanomedicine and Nanobiotechnology* **2009**, *2*, 99; c) K. Ulbrich, k. Hola, V. Subr, A. Bakandritsos, J. Tucek, R. Tucek, *Chem. Rev.* **2016,** *116*, 5338.

[20] a) H. X. Mai, Y. W. Zhang, R. Si, Z. G. Yan, L. D. Sun, L. P. You, C. H. Yan, *J. Am. Chem. Soc.* **2006**, *128*, 6426; b) J. C. Boyer, F. Vetrone, L. A. Cuccia, J. A. Capobianco, *J. Am. Chem. Soc.* **2006**, *128*, 7444.

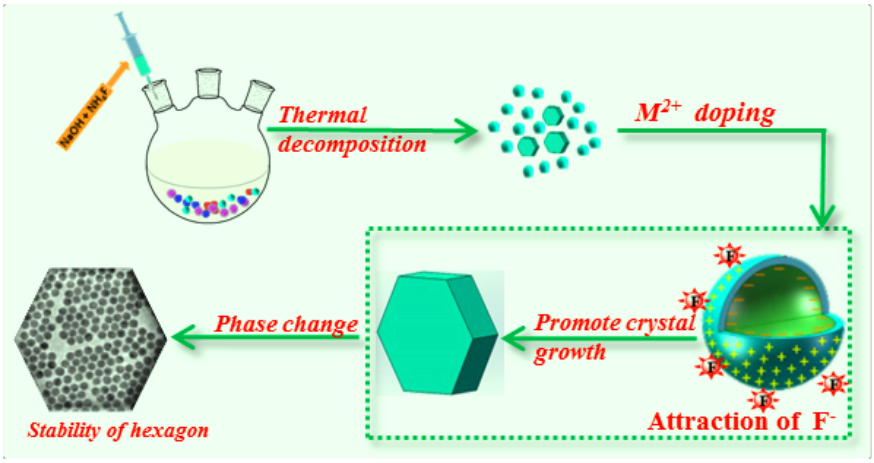

Scheme 1. Simplified schematic diagram of phase and size transition (cubic to hexagonal) mechanism of the $NaLnF_4$ UCNPs by doping M^{2+} ions (M= Mg, Co).

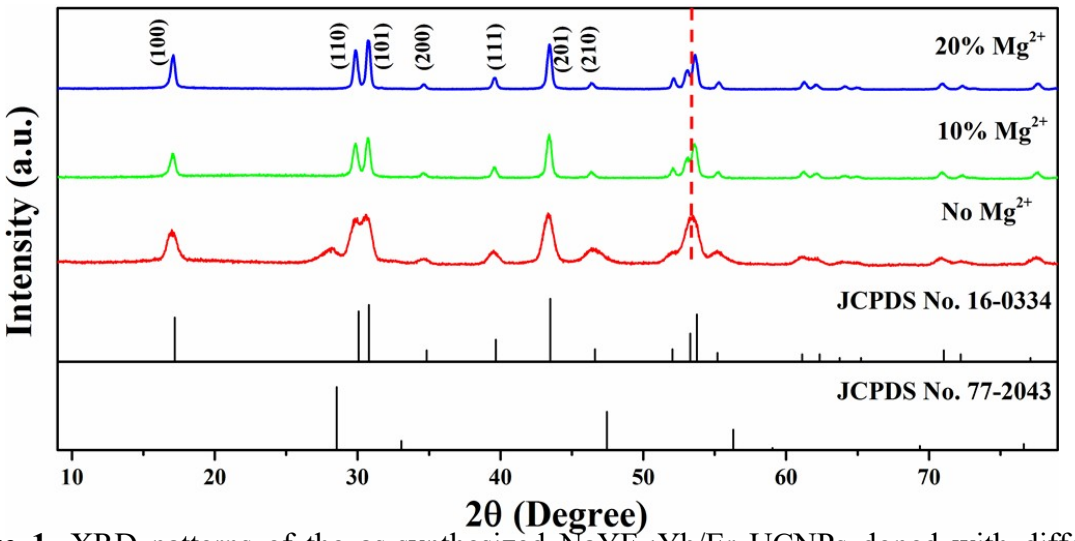

Figure 1. XRD patterns of the as-synthesized $NaYF_4$:Yb/Er UCNPs doped with different concentrations of Mg^{2+} at 0, 10, 20 mol%. The red dotted line indicates the diffraction peaks shift to high angel direction.

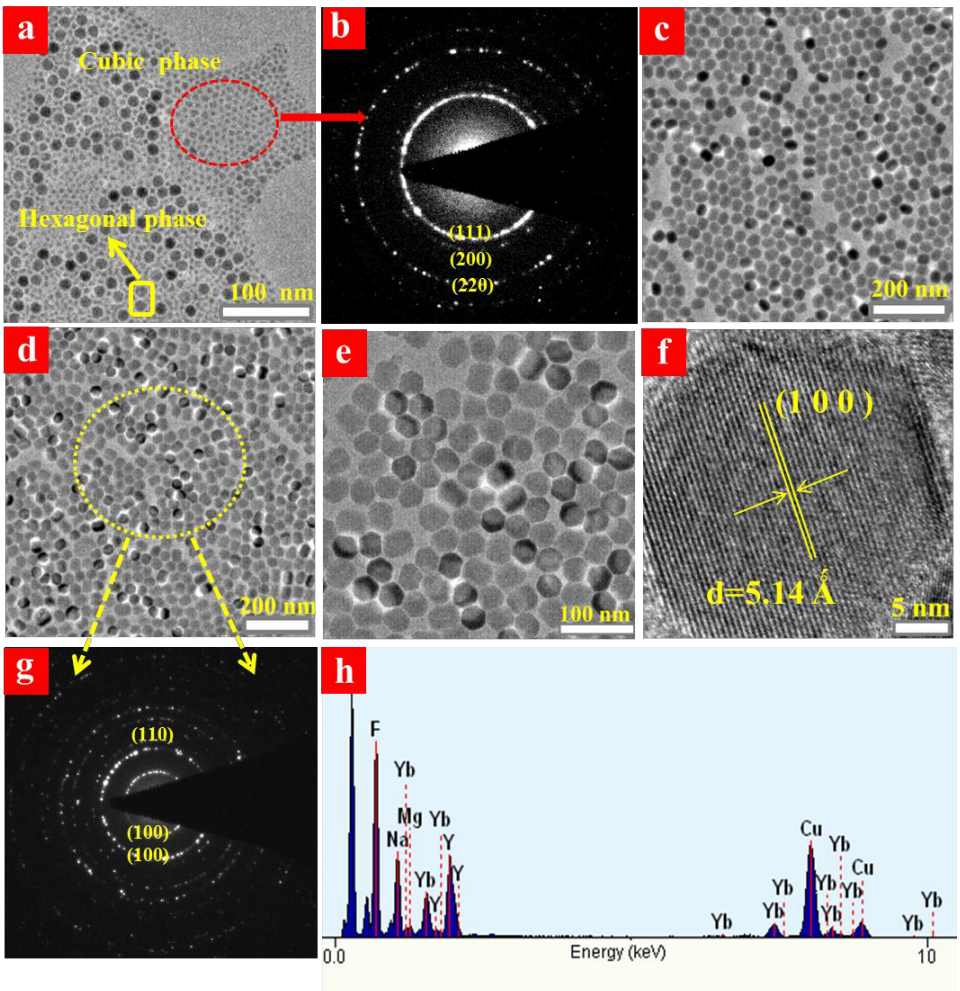

Figure 2. TEM images of $NaYF_4$:Yb/Er UCNPs doped with different contents of Mg^{2+}: (a) 0% Mg^{2+}; (b) SAED taken from ultra-small particles of (a); (c) and (d, e) present the UCNPs doped with 10 and 20 mol% Mg^{2+}, respectively; (f) and (g) are the corresponding HRTEM image of a single particle and SAED image taken from (d), respectively; (h) EDS pattern of the as-prepared $NaYF_4$: 20Yb/2Er/20Mg mol % UCNPs taken from (d).

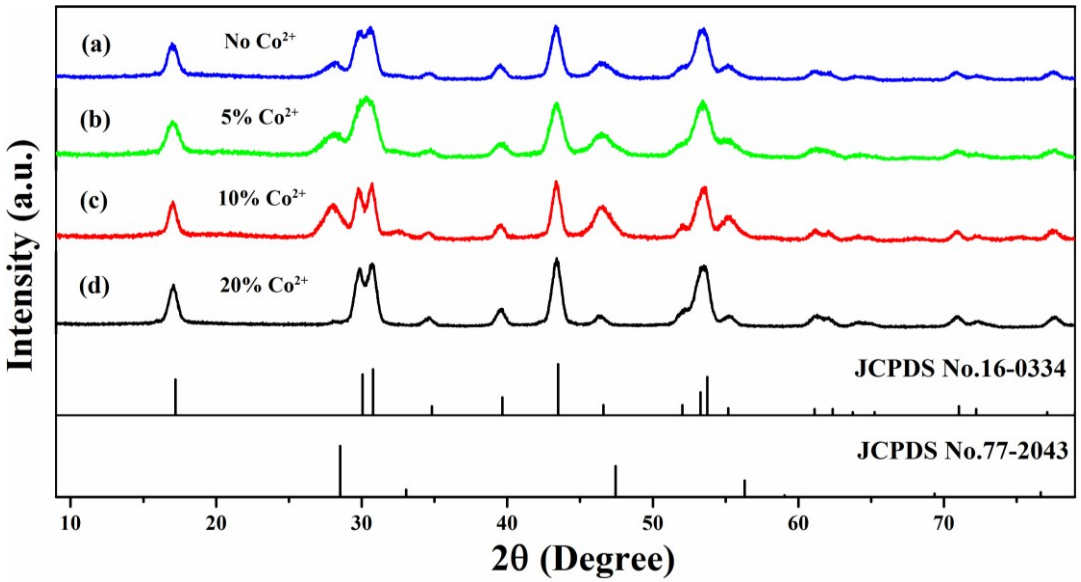

Figure 3. XRD patterns of the as-prepared $NaYF_4$ samples doped with different concentrations of Co^{2+}: (a) 0%, (b) 5%; (c) 10%; (d) 20%, respectively. The standard cards JCPDS No. 16-0334 (hexagonal phase) and JCPDS No. 77-2043 (cubic phase) were presented at the bottom.

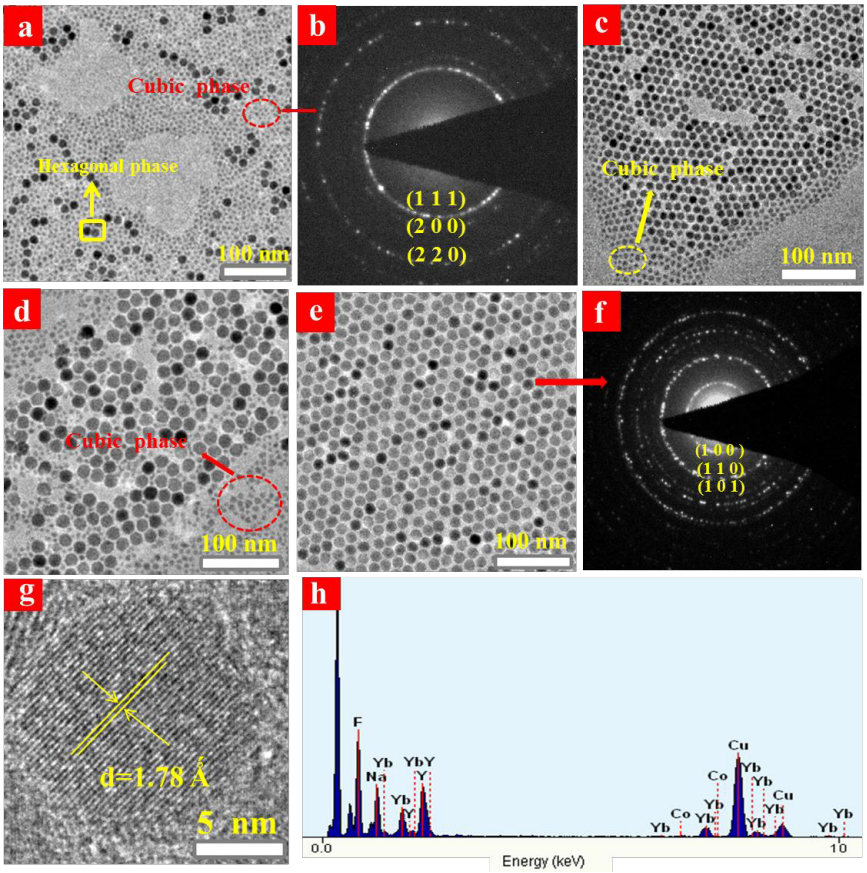

Figure 4. TEM images of $NaYF_4$ samples doped with different contents of Co^{2+}. (a), (c)-(e) were the typical TEM images of the $NaYF_4$:Yb/Er UCNPs doped with different concentrations of Co^{2+} (0, 5, 10, 20), respectively; (b) SAED image taken from (a); (f), (g), (h) were the SAED, HRTEM and EDS analysis of UCNPs taken from (e).

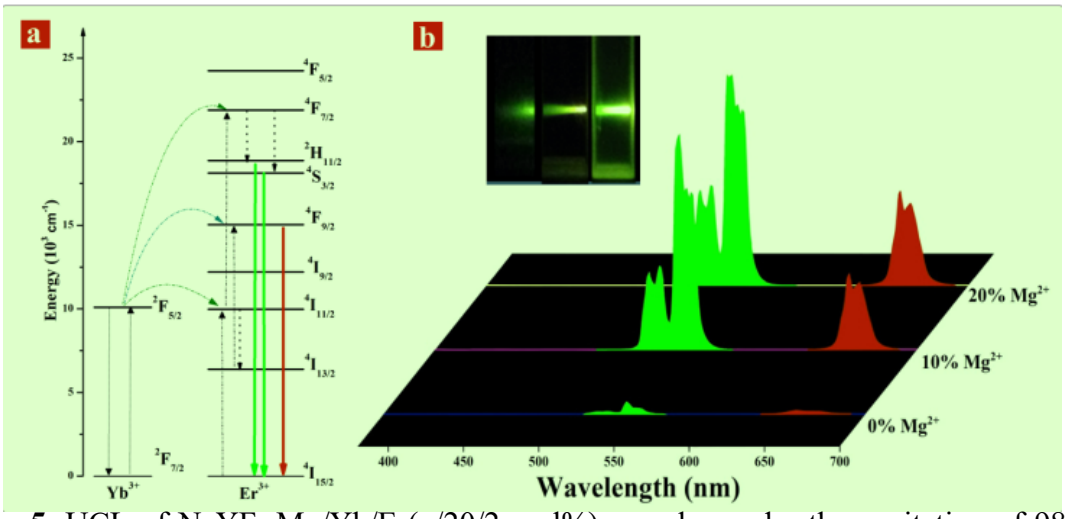

Figure 5. UCL of $NaYF_4$:Mg/Yb/Er(x/20/2 mol%) samples under the excitation of 980 nm laser. (a) Simplified energy level diagram, (b) UCL spectra of $NaYF_4$ UCNPs doped with different contents of Mg^{2+}, the inset of (b) shows the corresponding digital photos (from the left to the right) of $NaYF_4$:Yb/Er/xMg (x= 0, 10, 20) samples dissolved in 2 mL cyclohexane under the excitation of 980 nm laser.

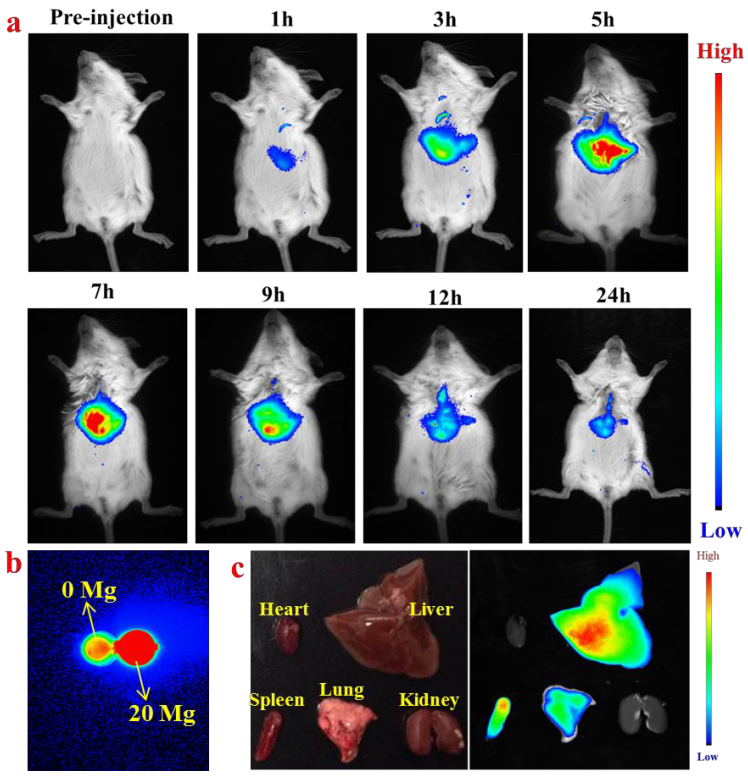

Figure 6. (a) *In vivo* UC optical imaging of a mouse after intravenously injected with 200 μL $NaYF_4$: 20Yb/ 2Er/20Mg mol % UCNPs at different time periods. (b) *In vitro* phantom imaging of a 96 well-plates separately filled with 300 μL of Mg-free $NaYF_4$ UCNPs and 20% Mg doped $NaYF_4$:Yb/Er UCNPs. (c) *Ex vivo* imaging of 20% Mg doped $NaYF_4$:Yb/Er UCNPs in isolated organs (heart, liver, spleen, lung, kidney) after 24 h injection.

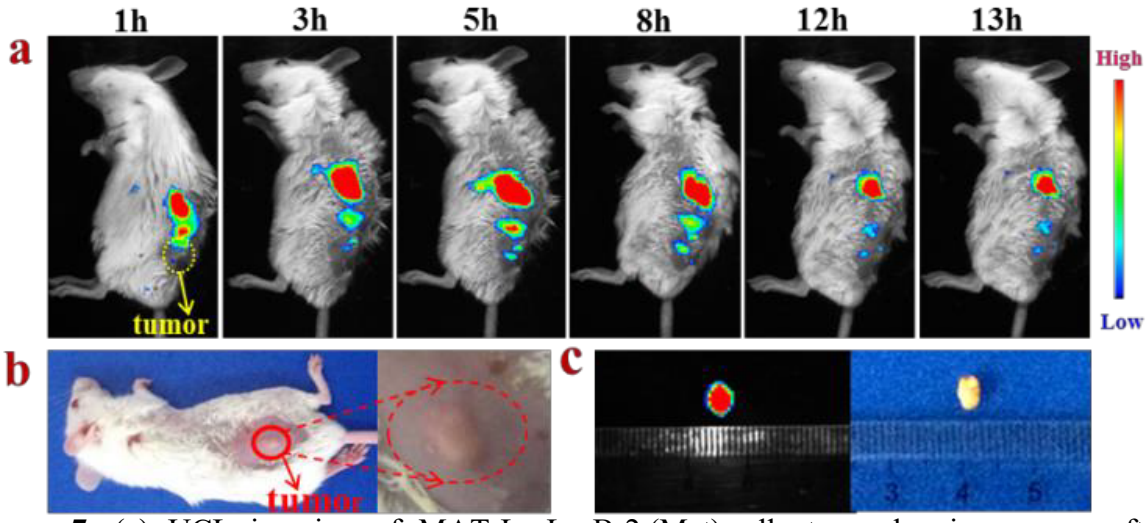

Figure 7. (a) UCL imaging of MAT-Ly-Lu-B-2 (Mat) cells tumor-bearing mouse after intravenously injected with hydrophilic-$NaYF_4$:20Yb/2Er/20Mg mol % UCNPs at different times, (b) in situ digital photo of the tumor, (c) *Ex-vivo* UCL bioimaging (left panel) and the digital photo (right panel) of the tumor.

A new strategy of M^{2+} doping method for simultaneous phase/size control and enhanced upconversion luminescence of $NaLnF_4$ UCNPs has been demonstrated. Moreover, red upconversion luminescence-guided tiny tumor diagnosis (3 mm) was successfully achieved. These findings open up a new way of designing high efficient upconversion luminescent probe with combination of hexagonal phase and small size for tiny tumor detection.

Keywords: M^{2+} doping, phase/size control, cubic to hexagonal phase transformation, optical-guided tiny tumor diagnosis

Youbin Li, Xiaolong Li, Zhenluan Xue, Mingyang Jiang, Songjun Zeng,* and Jianhua Hao*

M^{2+} doping induced simultaneous phase/size control and remarkable enhanced upconversion luminescence of $NaLnF_4$ probes for optical-guided tiny tumor diagnosis

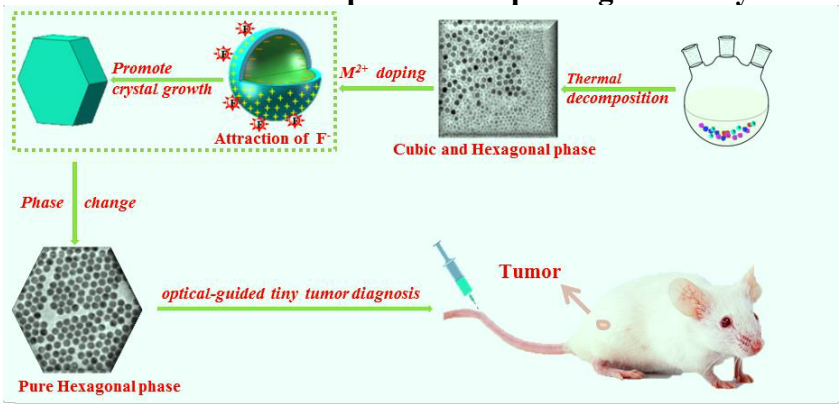

Supporting Information

M^{2+} doping induced simultaneous phase/size control and remarkable enhanced upconversion luminescence of $NaLnF_4$ probes for optical-guided tiny tumor diagnosis

Youbin Li, Xiaolong Li, Zhenluan Xue, Mingyang Jiang, Songjun Zeng, and Jianhua Hao**

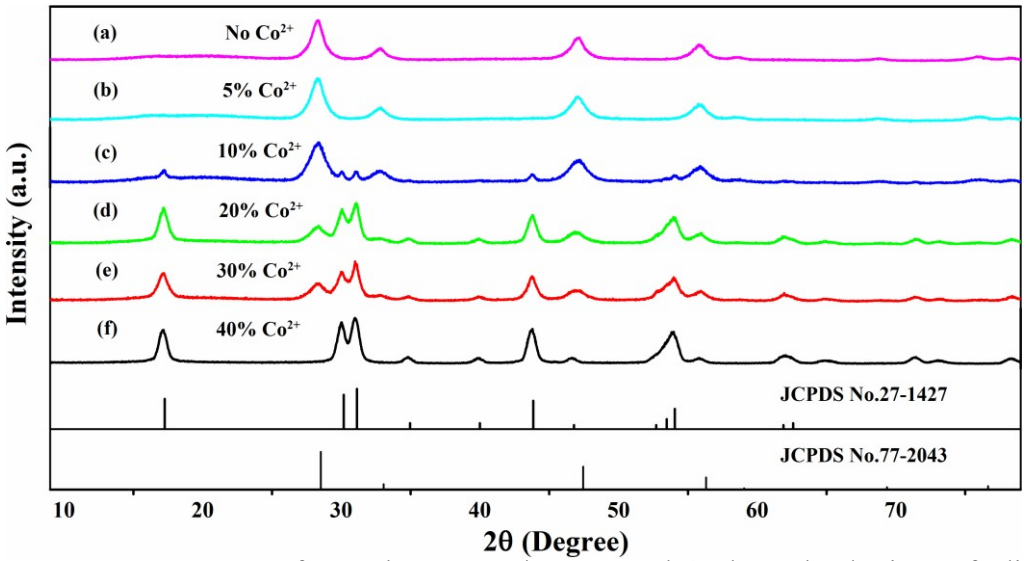

Figure S1. XRD patterns of $NaYbF_4$: 2Tm/ xCo mol% through doping of different concentrations of Co: (a) 0%, (b) 5%, (c) 10%, (d) 20%, (e) 30%, (f) 40%, respectively. The standard cards JCPDS No. 27-1427 (hexagonal phase) and JCPDS No. 77-2043 (cubic phase) were presented at the bottom.

Table S1. The quantitiy EDS result of $NaLnF_4$ UCNPs doped with different concentrations of M^{2+}

Doping concentration	Atomic percentage	
$NaYF_4$ host	Ln^{3+}	M^{2+}
10% mol Mg	90	7.0
20% mol Mg	88.7	11.3
5% mol Co	96.9	3.1
10% mol Co	95.4	4.6
20% mol Co	95.1	4.9
$NaYbF_4$ host		
10% mol Co	97.3	2.7
20% mol Co	91.2	8.8
30% mol Co	90.9	9.1
40% mol Co	86.3	13.7

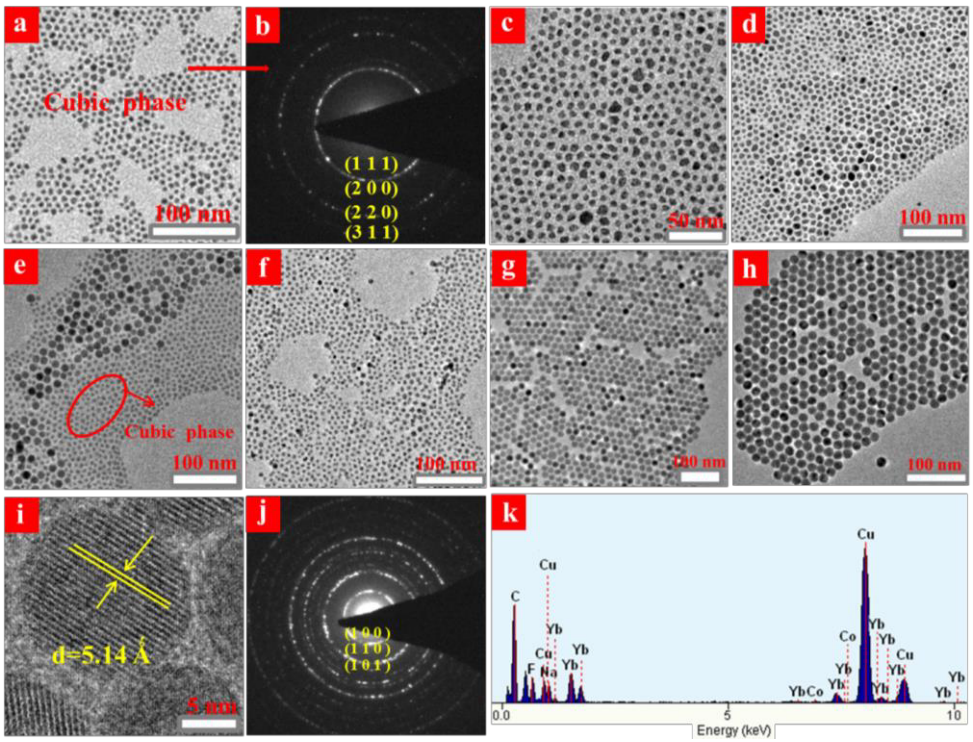

Figure S2. TEM images of $NaYbF_4$:Tm UCNPs doped with different contents of Co^{2+}: (a) 0%, (c) 5%, (d) 10% (e) 20%, (f) 30%, (g) and (h) 40%, respectively; (b) corresponding SAED pattern of (a); (i) HRTEM image of a single nanoparticle taken from (g). (j) The SAED pattern of nanoparticles taken from (g); (k) EDS result of the as-prepared 40% mol Co^{2+} doped $NaYbF_4$ UCNPs taken from (g).

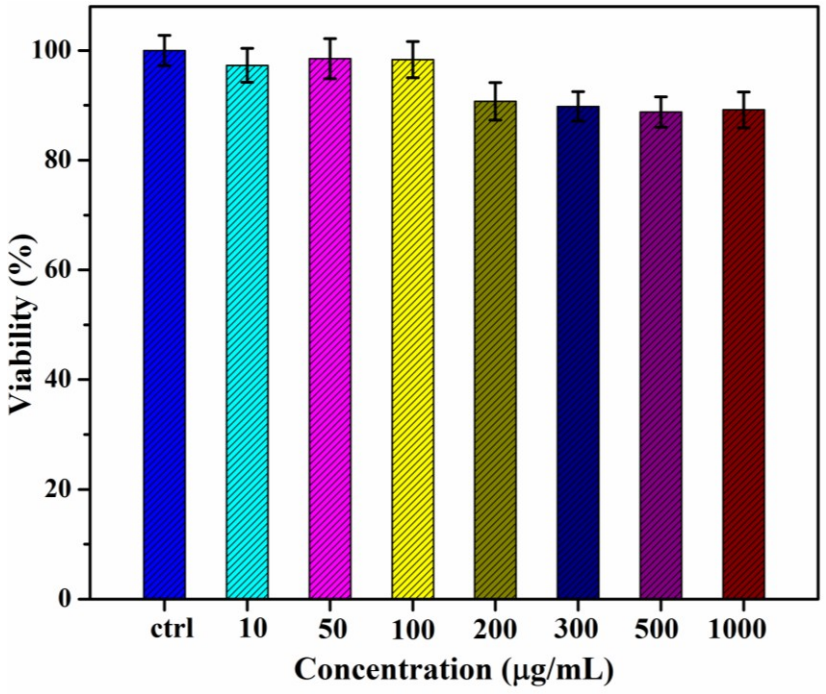

Figure S3. Cell toxicity test in HeLa cells treated with different concentrations of ligand-free $NaYF_4$:Yb/Er/Mg UCNPs at 37 ℃ for 24 h under 5% CO_2.